Archives of Biochemistry and Biophysics XX

Contents lists available at ScienceDirect

Archives of Biochemistry and Biophysics

journal homepage: www.elsevier.com/locate/yabbi

Early oxidative damage induced by doxorubicin: Source of production, protection by GKT137831 and effect on Ca^{2+} transporters in HL-1 cardiomyocytes

Mari C. Asensio-López [a], Fernando Soler [b], Jesús Sánchez-Más [a], Domingo Pascual-Figal [a, c], Francisco Fernández-Belda [b, *], Antonio Lax [a]

[a] Cardiología Clínica y Experimental, Departamento de Medicina Interna, Facultad de Medicina, Universidad de Murcia, Campus de El Palmar, 30120, Murcia, Spain
[b] Departamento de Bioquímica y Biología Molecular A, Universidad de Murcia, Campus de Espinardo, 30071, Murcia, Spain
[c] Servicio de Cardiología, Hospital Clínico Universitario Virgen de la Arrixaca, 30120, El Palmar, Murcia, Spain

ARTICLE INFO

Article history:
Received 19 November 2015
Received in revised form
4 February 2016
Accepted 18 February 2016
Available online XX

Keywords:
Doxorubicin
Reactive oxygen species
GKT137831
Ca^{2+} transporters
NADPH oxidase
Cardiotoxicity

ABSTRACT

In atrial-derived HL-1 cells, ryanodine receptor and Na^+/Ca^{2+}-exchanger were altered early by 5 μM doxorubicin. The observed effects were an increase of cytosolic Ca^{2+} at rest, ensuing ryanodine receptor phosphorylation, and the slowing of Ca^{2+} transient decay after caffeine addition. Doxorubicin triggered a linear rise of reactive oxygen species (ROS) with no early effect on mitochondrial inner membrane potential. Doxorubicin and ROS were both detected in mitochondria by colocalization with fluorescence probes and doxorubicin-induced ROS was totally blocked by mitoTEMPO. The NADPH oxidase activity in the mitochondrial fraction was sensitive to inhibition by GKT137831, and doxorubicin-induced ROS decreased gradually as the GKT137831 concentration added in preincubation was increased. When doxorubicin-induced ROS was prevented by GKT137831, the kinetic response revealed a permanent degree of protection that was consistent with mitochondrial NADPH oxidase inhibition. In contrast, the ROS induction by doxorubicin after melatonin preincubation was totally eliminated at first but the effect was completely reversed with time. Limiting the source of ROS production is a better alternative for dealing with oxidative damage than using ROS scavengers. The short-term effect of doxorubicin on Ca^{2+} transporters involved in myocardiac contractility was dependent on oxidative damage, and so the impairment was subsequent to ROS production.

1. Introduction

The cytosolic Ca^{2+} signal during sarcolemmal depolarization in mammalian atrial myocytes is originated by activation of the small population of junctional ryanodine receptor (RyR) around the periphery of the cell owing to the lack or poorly-developed T-tubules system. Accordingly, the Ca^{2+} signal does not fully spread inside the cell and the large population of non-junctional RyR remains inactive. Activation of non-junctional RyR occurs by successive processes of Ca^{2+}-induced Ca^{2+} release. This allows the enhancement of cardiac contractility and therefore the pumping of blood when positive inotropic agents promote Ca^{2+} propagation deep into the cell [1]. Differences in the expression, subcellular distribution and interaction with other proteins of a few key players, including RyR2, sarco-endoplasmic reticulum Ca^{2+}-ATPase (SERCA) 2a and Na^+/Ca^{2+}-exchanger (NCX) 1, are responsible for dissimilarities in Ca^{2+} signaling between atrial and ventricular myocytes [2].

On the other hand, the cardiotoxic effects attributed to doxorubicin can be classified as acute or chronic depending on whether a short- or long-term treatment is established [3]. The primary, but

Abbreviations used: RyR, ryanodine receptor; SERCA, sarco-endoplasmic reticulum Ca^{2+}-ATPase; NCX, Na^+/Ca^{2+}-exchanger; ROS, reactive oxygen species; AM, acetoxymethyl; H_2-DCFDA, 2′,7′-dichlorodihydrofluorescein diacetate; DCF, 2′,7′-dichlorofluorescein; SCT, spontaneous Ca^{2+} transient; *k*, apparent first-order rate constant for Ca^{2+} transient decay; Ru360, oxygen-bridged dinuclear ruthenium amine complex; a.u., arbitrary units; $\Delta\Psi_m$, mitochondrial inner membrane potential; CCCP, carbonyl cyanide *m*-chlorophenylhydrazone; GKT137831, 2-(2-chlorophenyl)-4-[3-dimethylamino)phenyl]-5-methyl-1*H*-pyrazolo[4,3-*c*]pyridine-3,6(2*H*,5*H*)-dione; NOX, NADPH oxidase.

* Corresponding author.
E-mail address: fbelda@um.es (F. Fernández-Belda).

http://XX
0003-9861/

not exclusive, cause of acute cardiotoxicity is related with an increase of reactive oxygen species (ROS). One-electron redox cycling of doxorubicin, supported by different enzymatic systems that can be potentiated by the iron released from intracellular stores, is the molecular mechanism responsible for ROS production [4]. Moreover, there is compelling evidence that the alteration of Ca^{2+} transporters is a key factor in doxorubicin-induced oxidative damage. It has been described that the inhibition of Ca^{2+} entry through NCX [5], the increase in RyR open probability [6], the activation of L-type cardiac Ca^{2+} channels [7] and the down-regulation of genes related with sarcoplasmic reticulum Ca^{2+} transporters [8] among others are linked to the increased production of ROS evident upon doxorubicin exposure.

The cardiomyocyte is especially sensitive to oxidative damage due to the high mitochondrial content and the low antioxidant defenses, therefore the presence of doxorubicin as a potent source of ROS is expected to have great impact. Since doxorubicin was demonstrated to alter intracellular Ca^{2+} transporters and Ca^{2+} signaling is different in atrial and ventricular myocytes [9] it was considered of interest to explore the effect of doxorubicin on atrial muscle cells.

HL-1 is a cell line that continuously proliferates, contracts and retains several phenotypic characteristics of cardiomyocytes when cultured *in vitro* [10]. The cells are endowed with highly ordered myofibrils, cardiac-specific junctions, voltage dependent currents, the expression of sarcoplasmic reticulum Ca^{2+} transport proteins as well as Ca^{2+} transients in response to caffeine or electrical field stimulation [10,11].

In the present study, HL-1 was used as a cellular model to analyze the effect of a short doxorubicin treatment on the Ca^{2+} transporters related with myocardial contractility in order to ascertain the source and localization of the oxidative damage and whether blunted oxidative damage is a mechanism accounting for full protection.

2. Materials and methods

2.1. Reagents and other products

Culture reagents including Claycomb medium, fetal bovine serum, L-glutamine, penicillin–streptomycin mixture and norepinephrine bitartrate (A0937) were obtained from Sigma-Aldrich. MitoTEMPO, lucigenin and NADPH were purchased from Santa Cruz Biotechnology and Fluo-3/acetoxymethyl (AM), 2′,7′-dichlorodihydrofluorescein diacetate (H_2-DCFDA), MitoTracker Green FM and JC-1 were Molecular Probes® products from Life Technologies-Invitrogen. GKT137831 was provided by BioVision. Pierce® BCA protein assay kit was from Thermo Fisher Scientific, protease inhibitor cocktail (P8340) was from Sigma and Calbiochem® phosphatase inhibitor cocktail set II (524625) was from Merck Millipore. Primary antibodies against RyR2 phosphorylated at Ser2808 (A010-30) or phosphorylated at Ser2814 (A010-31) were obtained from Badrilla whereas unphosphorylated anti-RyR2 (MA3-925) was from Pierce® Thermo Scientific. Secondary antibody peroxidase-conjugated anti-rabbit IgG (W401-B) was from Promega. Immobilon®-PSQ membrane for electroblotting was from Merck Millipore. Horseradish peroxidase activity was detected with the Amersham™ ECL Prime reagent from GE Healthcare and ChemiDoc XRS+ system from BioRad. Quantitative analysis was carried out with Gel-Pro Analyzer 3.1 software from Sigma. All other reagents were also supplied by Sigma-Aldrich.

2.2. Cell culture and doxorubicin treatment

Cells in complete culture medium consisting of Claycomb medium, 10% heat-inactivated fetal bovine serum, 2 mM L-glutamine, 100 U/ml penicillin, 100 μg/ml streptomycin and 0.1 mM norepinephrine were maintained at 37 °C in exponential growth phase. The monolayer culture was split in a 1:6 ratio or harvested to perform experiments when confluence was 70–80%. Fetal bovine serum, antibiotics and norepinephrine were removed from the medium 12 h before measurements. For the induction of cardiotoxicity, plated cells were exposed to 5 μM doxorubicin for the indicated incubation times. The doxorubicin concentration was selected according to previous assays and reproduces the plasma peak concentration reached by standard infusion in patients [12,13].

2.3. Measurement of cytosolic Ca^{2+}

Free Ca^{2+} concentration was measured as described previously [14]. Briefly, subconfluent cultures were loaded in the dark at 37 °C for 30 min with 2 μM Fluo-3/AM in Tyrode medium containing 10 mM Hepes, 150 mM NaCl, 5.4 mM KCl, 1.2 $MgCl_2$, 1.8 mM $CaCl_2$, 10 mM glucose, 0.9 mM NaH_2PO_4 and 0.25% bovine serum albumin adjusted to pH 7.4 with NaOH. Extrusion of the free acid-Ca^{2+} probe was prevented by including 0.2 mM sulfinpyrazone. Loading was followed by 30 min deesterification. Fluorescence emission was captured with Leica equipment consisting of a TCS SP2 scanhead module coupled to an inverted microscope (DM IRE II). The oil immersion objective was HCX PL APO 63x and the confocal section 1.1 μm. Time-dependent images were collected with a Leica DC300 FX digital camera using the customized software IM50 1.2. Samples at room temperature were excited with the 488 nm argon-ion laser line and the green fluorescence was observed in the 504–530 nm wavelength range. Cells in the field were repetitively scanned at 1 s intervals for a total duration of 15 min. Calibration was performed at the end of each experiment by adding 1 μM ionomycin to determine F_{max} and 40 mM EGTA aliquots until fluorescence no longer diminished to determine F_{min}. Cytosolic free Ca^{2+} was calculated according to the Grynkiewicz equation [15]. The apparent dissociation constant for the Ca^{2+}-Fluo-3 complex was 390 nM.

2.4. Ca^{2+} extrusion transporters

The relative contribution to cytosolic Ca^{2+} removal was estimated from the apparent first-order rate constant of Ca^{2+} transient decay [16,17]. Plated cells displayed spontaneous Ca^{2+} transients (SCT) and were used to determine the rate constant of the corresponding Ca^{2+} transient decay (k_{SCT}). Moreover, the rate constant of Ca^{2+} transient decay induced by caffeine (k_{Caff}) was obtained by adding 10 mM caffeine. When the rate constant of Ca^{2+} transient decay was measured in the presence of Ni^{2+} ($k_{Caff+Ni}$), cells were preincubated with 10 mM $NiCl_2$ before the addition of 10 mM caffeine. Likewise, the rate constant of Ca^{2+} transient decay in the presence of Ni^{2+} and oxygen-bridged dinuclear ruthenium amine complex (Ru360) ($k_{Caff+Ni+Ru}$) was obtained when cells were preincubated with 10 mM $NiCl_2$ plus 10 μM Ru360 and 10 mM caffeine was added. SCT in individual cells or caffeine-induced Ca^{2+} discharges in random cell fields were analyzed by confocal microscopy after loading the cells with Fura-3/AM and maintaining in Tyrode medium.

2.5. Detection of phosphorylated RyR2

Cells in subconfluent cultures (~6×10^6 cells) were exposed or not to 5 μM doxorubicin for different time intervals. Thereafter, each plate was washed twice with phosphate-buffered saline at 4 °C and exposed to 100 μl of ice-cold solubilization medium

containing 20 mM Tris-HCl, pH 7.4, 150 mM NaCl, 50 mM NaF, 1% (w/v) Nonidet P-40, 1% (w/v) sodium deoxycholate, 0.1% (v/v) SDS, 2 mM EDTA, 10% (v/v) glycerol, 5 mM sodium orthovanadate, 1 mM phenylmethanesulfonyl fluoride, 1% (v/v) protease inhibitor cocktail and 1% (v/v) phosphatase inhibitor cocktail. The cells were gently scraped from the plate, transferred to an Eppendorf tube and maintained on an ice-water bath for 30 min. During this time, the suspension was vortexed for 10 s intervals every 5 min. Samples were subjected to centrifugation at 10,000× *g* for 20 min and 4 °C and the supernatant containing solubilized proteins was aliquoted and stored at −80 °C for further use. Ninety μg of protein per lane were electrophoresed on 6% SDS-polyacrylamide minigels and electroblotted on polyvinylidene difluoride membranes for immunological detection [18]. The proteins of interest were probed at 1:5000 dilution with anti-phosphoSer2808 RyR2, anti-phosphoSer2814 RyR2 or unphosphorylated RyR2.

2.6. Production of ROS

Doxorubicin-induced ROS was measured with the aid of the cell-permeable indicator H_2-DCFDA [19]. After intracellular deacetylation, the non-fluorescent dye 2′,7′-dichlorodihydrofluorescein was oxidized by ROS to the fluorescent 2′,7′-dichlorofluorescein (DCF). Cells in a 96-well microtiter plate were grown at 37 °C for 2 days in complete culture medium to obtain ~8 × 10^4 cells/well. These were then washed with prewarmed phosphate-buffered saline and loaded in the dark at 37 °C for 30 min with 10 μM H_2-DCFDA in Claycomb medium. Excess probe was washed off and cells in Tyrode medium were maintained at 25 °C for 20 min before measurements. The increase in DCF fluorescence induced by doxorubicin was expressed in arbitrary units (a.u.) or a.u./min with respect to a control in the absence of drug. Cells in the presence of 5 μM doxorubicin were used to subtract the drug absorbance and/or autofluorescence as described previously [18]. The time-dependent appearance of green fluorescence was monitored at excitation and emission wavelengths of 485 and 530 nm, respectively using a Fluostar Omega microplate reader (BMG Labtech).

2.7. Mitochondrial inner membrane potential ($\Delta\Psi_m$)

Polarized mitochondria exhibit red fluorescence when exposed to the carbocyanine dye JC-1 due to the accumulation of J-aggregates [20]. Cells in a 96-well microtiter plate were grown at 37 °C for 2 days in complete culture medium to reach ~8 × 10^4 cells/well. They were then washed with prewarmed phosphate-buffered saline and loaded at 37 °C for 15 min with 5 μg/ml JC-1. After two wash cycles with phosphate-buffered saline, cells in Tyrode medium were subjected to the corresponding treatment. The green fluorescence of monomeric JC-1 and the red fluorescence of aggregate JC-1 were recorded as a function of time using a Fluostar Omega microplate reader. Excitation was fixed at 490 nm and the emission was alternately collected at 530 and 590 nm. Data are expressed as ratio of red/green fluorescence after correction for doxorubicin autofluorescence and/or energy transfer to JC-1.

2.8. Intracellular localization of doxorubicin and ROS

The presence of doxorubicin inside the cell was monitored using the red fluorescence of the molecule and the mitochondrial probe MitoTracker Green as a reference. Subconfluent cultures in 35-mm glass bottom plates were washed twice with phosphate-buffered saline at 37 °C. Then, cells were incubated at 37 °C in prewarmed Tyrode medium with 150 nM MitoTracker Green for 20 min in the dark. After loading, the cells at 37 °C were washed twice before exposure to 5 μM doxorubicin for the indicated times. Cells were examined at different time intervals by laser scanning confocal microscopy using the above described Leica equipment. MitoTracker Green and doxorubicin were excited with the 488 nm line of the argon-ion. The emission fluorescence was selected in the wavelength range 500–540 nm for MitoTracker Green or 620–700 nm for doxorubicin. The intracellular distribution of ROS was followed by the fluorescence associated to DCF using the doxorubicin red fluorescence as a marker. For these assays, cells in 35-mm glass bottom plates were incubated at 37 °C in the dark with 5 μM doxorubicin. After loading, the cells were washed twice with prewarmed phosphate-buffered saline before exposure at 37 °C to 10 μM H_2-DCFDA in Claycomb medium. DCF and doxorubicin were excited with the 488 nm line of the argon-ion laser and the emission fluorescence was collected at 500–530 nm for DCF or 620–700 nm for doxorubicin.

2.9. Fluorescence quantitative colocalization

Correlation of the pixel intensities between the two color channels was carried out by the Pearson correlation and Manders overlap coefficients [21]. The first ranges from −1 for complete exclusion to +1 for complete correlation, whereas the second varies from 0 for no colocalization to 1 for full colocalization. High magnification images of 1024 × 1024 pixels were collected and a number of cytoplasmic regions of interest in individual cells (n) were selected. Image processing and analysis were performed with the public domain software Fiji (http://fiji.sc/Fiji) and the JACoP v2.0 Plugin (http://rsb.info.nih.gov/ij/plugins/track/jacop.html).

2.10. Subcellular fractions

Subconfluent cultures harvested with trypsin/EDTA and pooled in Eppendorf tube (~24 × 10^6 cells) were washed twice with phosphate-buffered saline at 4 °C. Afterwards, cells resuspended in 400 μl of ice-cold medium containing 8 mM Na_2HPO_4, 1 mM NaH_2PO_4, 75 mM KCl and 250 mM sucrose adjusted to pH 7.0 were lysed on an ice-water bath with 80 strokes in a glass-teflon Dounce homogenizer. After centrifugation at 10,000× *g* for 20 min and 4 °C, the supernatant was saved as the microsomal + cytosolic fraction and stored at −80 °C for further use. The resulting pellet, once resuspended in 400 μl of ice-cold medium containing 50 mM KH_2PO_4 and 1 mM EGTA at pH 7.0, was vigorously vortexed 5 times (10 s each time), maintaining the samples for 5 min intervals on an ice-water bath. This provided the mitochondrial fraction that was stored at −80 °C until use.

2.11. NADPH oxidase (NOX) activity

NOX activity in subcellular fractions was evaluated in the presence of lucigenin by chemiluminescence assay [22]. The enzyme reaction was measured at 25 °C in a 96-well microtiter plate. The initial assay medium was 50 mM KH_2PO_4, pH 7.0, 1 mM EGTA, 150 mM sucrose, 100 μM NADPH and 25 μM lucigenin. In a final volume of 0.2 ml, the reaction was started by adding 200 μg protein from the mitochondrial fraction or 400 μg protein from the microsomal + cytosolic fraction. Different concentrations of GKT137831 were present when indicated. The photon emission in each well was measured every 15 s for a period of 4 min using a Fluostar Omega microplate reader. Preliminary experiments were conducted to ensure a linear rate of lucigenin reduction and the absence of activity when NADPH was not included.

2.12. Protein determination

The protein concentration in cellular extracts and isolated

fractions was evaluated with the Pierce® bicinchoninic acid assay kit and bovine serum albumin as standard protein.

2.13. Data presentation

Cell images were representative of randomly selected fields and were reproduced using Adobe Photoshop 4.0 software. Representative or average traces of repeated experiments using more than one cell culture are given. The k values for Ca^{2+} transient decay correspond to the mean of a number of determinations (n) ± SEM. Data points and histogram bars are mean values of at least five independent assays and SEM is expressed by the error bar. p values were calculated by the Student's t-test using version 11.0 of the SigmaPlot program from Systat Software.

3. Results

3.1. Ca^{2+} transporters and doxorubicin effect

When plated cells at 70–80% confluence were incubated in resting conditions, confocal Ca^{2+} imaging in a field of Fluo-3 loaded cells showed occasional flashes of green fluorescence (Fig. 1A). In the absence of external Ca^{2+} entry, this spontaneous short-lived fluorescence or SCT can be attributed to discharge/sequestration of intracellular Ca^{2+}. The mean cytosolic Ca^{2+} signal in a single cell (n = 6) indicated that resting free Ca^{2+} was 70 nM, the Ca^{2+} peak amplitude was 660 nM and k_{SCT} was 508 ± 24 ms^{-1} (Fig. 1B). Average Ca^{2+} transients in random fields (n = 10) were also obtained when 10 mM caffeine was added to provoke irreversible Ca^{2+} discharge from the sarcoplasmic reticulum (Fig. 1C). In this case, the caffeine-induced Ca^{2+} peak amplitude was close to 1000 nM and k_{Caff} was 152 ± 16 ms^{-1}. When cells were preincubated for 10 min with 10 mM $NiCl_2$ to inhibit NCX before the addition of 10 mM caffeine (n = 8), $k_{Caff+Ni}$ was 59 ± 5 ms^{-1}. Moreover, when the preincubation was carried out in the presence of 10 mM $NiCl_2$ and 10 μM Ru360 to inhibit NCX and the mitochondrial Ca^{2+} uniporter (n = 8), $k_{Caff+Ni+Ru}$ was 52 ± 3 ms^{-1}. From these data the proportion of cytosolic Ca^{2+} removed by different Ca^{2+} transporters can be derived. The contribution of SERCA, i.e., Ca^{2+}-pumped inside the sarcoplasmic reticulum, was 70% as deduced from the expression $k_{SCT} - k_{Caff}/k_{SCT}$, whereas the fraction taken by the sarcolemmal NCX operating in the forward direction ($1Ca^{2+}_{out}$:$3Na^{+}_{in}$), calculated from $k_{Caff} - k_{Caff+Ni}/k_{SCT}$, was 18%. Cytosolic Ca^{2+} removed by the mitochondrial Ca^{2+} uniporter ($k_{Caff+Ni} - k_{Caff+Ni+Ru}/k_{SCT}$) was ~1% and the rest corresponds to other slow Ca^{2+} transporters (Fig. 1D).

The effect of doxorubicin on Ca^{2+} transporters was then analyzed during a 3 h test period by studying the evolution of the caffeine-induced Ca^{2+} transient. The time-dependent effect of 5 μM doxorubicin altered the resting Ca^{2+} level, Ca^{2+} peak amplitude and the kinetics of Ca^{2+} transient decay (Fig. 2A). The resting Ca^{2+} level remained unaffected for the first 30 min but increased as the treatment was prolonged (Fig. 2B), whereas the Ca^{2+} peak amplitude induced by caffeine displayed the opposite behavior, i.e., it was unaltered during the initial period of time but tended to decrease as the treatment was prolonged (Fig. 2C). The observed effects are consistent with increased diastolic Ca^{2+} efflux from the sarcoplasmic reticulum, commonly termed sarcoplasmic reticulum Ca^{2+} leak, and may involve activation of the RyR2 channel [23]. Therefore, the time-dependent effect of 5 μM doxorubicin on RyR2 activation was studied using Western blot and phospho-specific antibodies. RyR2 was not phosphorylated at Ser2808 over a period of 6 h when doxorubicin was added, although early phosphorylation at the protein kinase A-specific site Ser2808 was observed in the presence of 1 μM isoproterenol (Fig. 2D). Furthermore, significant phosphorylation of RyR2 at Ser2814 was evident following 15 min of doxorubicin treatment, and maintained for up to 6 h.

Since the kinetics of Ca^{2+} transient decay induced by caffeine in cells exposed to doxorubicin was delayed in a time-dependent manner, we next sought to ascertain whether or not NCX was affected. To this end, plated cells were exposed to 5 μM doxorubicin for 1 h and then 10 mM caffeine was added to induce the Ca^{2+} transient (n = 8). Alternatively, 10 mM $NiCl_2$ was added in preincubation before the 1 h doxorubicin treatment and the caffeine-induced Ca^{2+} transient was elicited (n = 8). Evaluation of the mono-exponential Ca^{2+} transient decay after the doxorubicin treatment indicated that k_{Caff} was 18 ± 3 ms^{-1} (Fig. 3, *top*), whereas $k_{Caff+Ni}$ was 9 ± 1 ms^{-1} (Fig. 3, *bottom*). The rate constant of the NCX activity assessed from the difference $k_{Caff} - k_{Caff+Ni}$ was 100 ms^{-1} in untreated cells (see Fig. 1C) and 9 ms^{-1} in cells exposed to 5 μM doxorubicin for 1 h (Fig. 3).

3.2. Doxorubicin relationship with mitochondria

Since doxorubicin is a potent inducer of oxidative damage the process of ROS formation was first characterized. Plated cells loaded with H_2-DCFDA responded with a linear increase of green fluorescence when 5 μM doxorubicin was added. This increase in fluorescence was observed from the initial time point (Fig. 4A) and linearity between DCF accumulation and doxorubicin concentration was confirmed (Fig. 4A, *inset*). Because the mitochondrion is a primary site of ROS production but it is also the target of oxidative damage, the potential relationship between doxorubicin and $\Delta\Psi_m$ was explored. In these experiments, plated cells in the absence of doxorubicin displayed intense red/green fluorescence when loaded with JC-1 that is indicative of high $\Delta\Psi_m$. Moreover, $\Delta\Psi_m$ remained unaltered during the time window of our experiment when cells were exposed to 5 μM doxorubicin (Fig. 4B), however when 5 μM CCCP was added a time-dependent loss of $\Delta\Psi_m$ was triggered.

The time course of doxorubicin entry inside the cell was monitored from the red fluorescence of the molecule. In the absence of doxorubicin, plated cells loaded with MitoTracker Green displayed green fluorescence (Fig. 5A). However, when cells were exposed to 5 μM doxorubicin a red fluorescence appeared at 15 min, the intensity and extension of which increased as a function of time. Exposure times longer than 1 h were needed to observe red fluorescence in the nuclei (data not shown). The yellow color in overlaid images was consistent with the mitochondrial localization of doxorubicin and was confirmed when viewed in more detail. Both mitochondrial probe and doxorubicin exhibited a punctate cytoplasmic distribution and were clearly superimposed (Fig. 5B). Analysis of fluorescence colocalization provided a Pearson coefficient of 0.87 ± 0.03 and Manders coefficient of 0.98 ± 0.01 (n = 5). Likewise, the ROS-induced green fluorescence of DCF and the intrinsic red fluorescence of doxorubicin largely overlapped, which is consistent with preferential ROS localization in the mitochondria. Pearson and Manders coefficients were calculated to be 0.86 ± 0.02 and 0.98 ± 0.01 (n = 10), respectively. When cells were preincubated with mitoTEMPO [24] for 1 h, the linear rate of DCF accumulation in the presence of 5 μM doxorubicin decreased in a concentration-dependent manner and was totally abolished when the mitochondrial antioxidant reached 50 μM (Fig. 5C).

3.3. Source of doxorubicin-induced ROS and protection

The NOX activity catalyzes one-electron transfer from NADPH to O_2 to give the free radical superoxide and has been implicated in physiological and pathological processes of ROS production. The potential relationship between NOX and doxorubicin-induced ROS

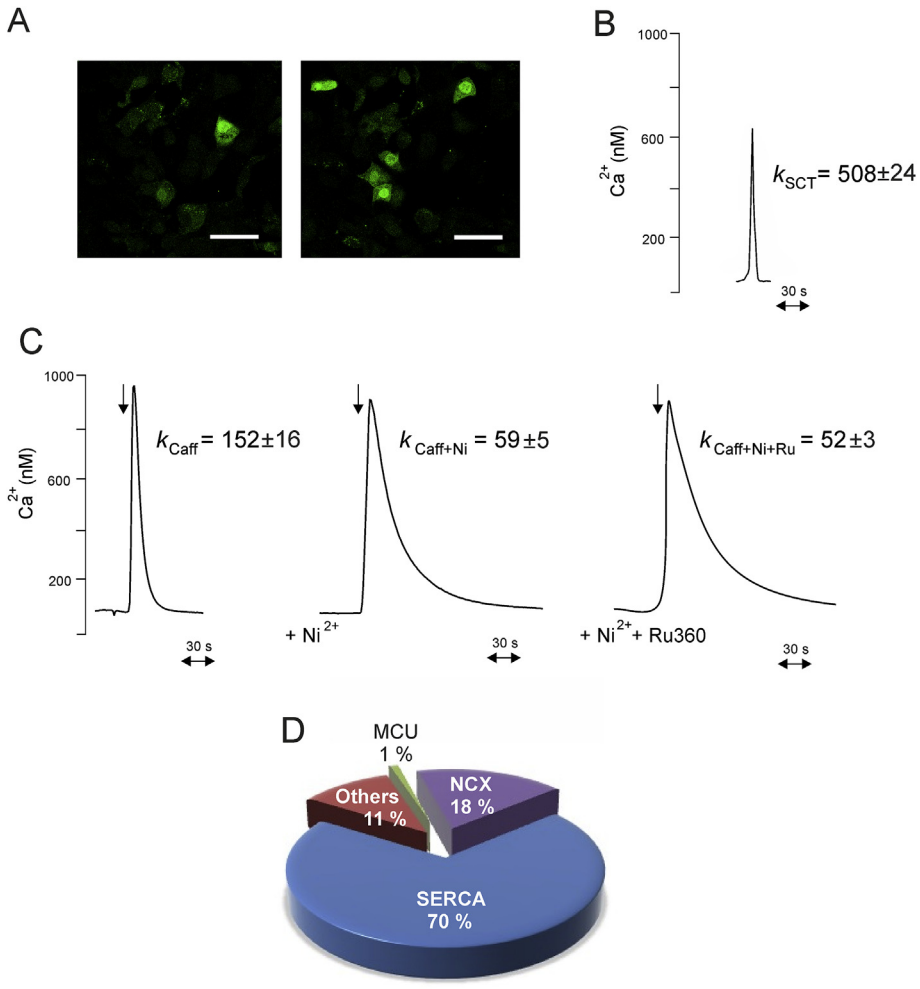

Fig. 1. Ca^{2+} transporters involved in cytosolic Ca^{2+} removal. Plated cells were loaded with Fura-3/AM and maintained in Tyrode medium during the experiments. (A) Confocal Ca^{2+} images taken from a sequence in a cell field where aleatory SCT can be observed. Bar length is 50 μm. (B) Average fluorescence trace of SCT in single cell used to determine the rate constant of Ca^{2+} transient decay (k_{SCT}). (C) Average fluorescence traces of cytosolic Ca^{2+} when cells were exposed to 10 mM caffeine (arrow) to provoke irreversible discharge of the sarcoplasmic reticulum Ca^{2+} store. The decay phase was used to determine k_{Caff}. When cells were preincubated for 5 min with 10 mM $NiCl_2$ or 10 mM $NiCl_2$ plus 10 μM Ru360 the decay phase of the caffeine-induced Ca^{2+} transient was used to evaluate $k_{Caff+Ni}$ or $k_{Caff+Ni+Ru}$, respectively. First-order rate constants for Ca^{2+} transient decays are expressed in ms^{-1}. (D) Pie chart showing relative contribution of cytosolic Ca^{2+} transporters. MCU is mitochondrial Ca^{2+} uniporter.

in HL-1 cells was first approached by evaluating the *in vitro* NOX activity in the relevant subcellular fractions. Our data indicated that NOX activity was present in the mitochondrial but not in the microsomal + cytosolic fraction. Moreover, NOX activity in the mitochondrial fraction was progressively inhibited when the concentration of the selective NOX inhibitor GKT137831 was raised (Fig. 6A). Full inhibition was attained at approximately 1 μM. Then, the generation of doxorubicin-induced ROS was examined by including a preincubation step with the NOX inhibitor. Thus, plated cells were preincubated or not for 1 h with GKT137831 before the addition of 5 μM doxorubicin. As can be seen, the DCF fluorescence rate gradually diminished as the GKT137831 concentration added in preincubation was raised. Total inhibition required the presence of approximately 3 μM (Fig. 6B).

To further explore the mechanism of protection we studied the time-dependent response of doxorubicin-induced ROS when cells were subjected to 15 min preincubation with the NOX inhibitor GKT137831 or the ROS scavenger melatonin. The linear rate of DCF accumulation gradually decreased as the GKT137831 concentration added in preincubation was increased (Fig. 7A). Nonetheless, the DCF accumulation was totally eliminated by melatonin preincubation, even at the lower concentrations tested, although the protection was temporary (Fig. 7B). The kinetic response was characterized by the appearance of a time lag that increased in length as the melatonin concentration was raised from 10 to 100 μM.

3.4. Protection of Ca^{2+} transporters

The relationship between doxorubicin-dependent ROS and the alteration of Ca^{2+} transporters involved in myocardiac contractility was then addressed by measuring the caffeine-induced Ca^{2+} transient in the presence of the above-mentioned compounds that prevented the formation or avoided the accumulation of ROS. The Ca^{2+} transient induced by 10 mM caffeine showed the characteristic decrease in peak amplitude and slower transient decay after 1 h treatment with 5 μM doxorubicin (Fig. 8, *trace a*), as already shown in Fig. 2A. However, the caffeine-induced Ca^{2+} signal remained unaltered after doxorubicin treatment when cells were preincubated with 3 μM GKT137831 (n = 3), 50 μM mitoTEMPO (n = 3) or 100 μM melatonin (n = 3) (Fig. 8, *traces b-d*). In terms of the caffeine-induced Ca^{2+} transient decay, the doxorubicin treatment did not decrease k_{Caff} when cells were preincubated before with the above mentioned compounds.

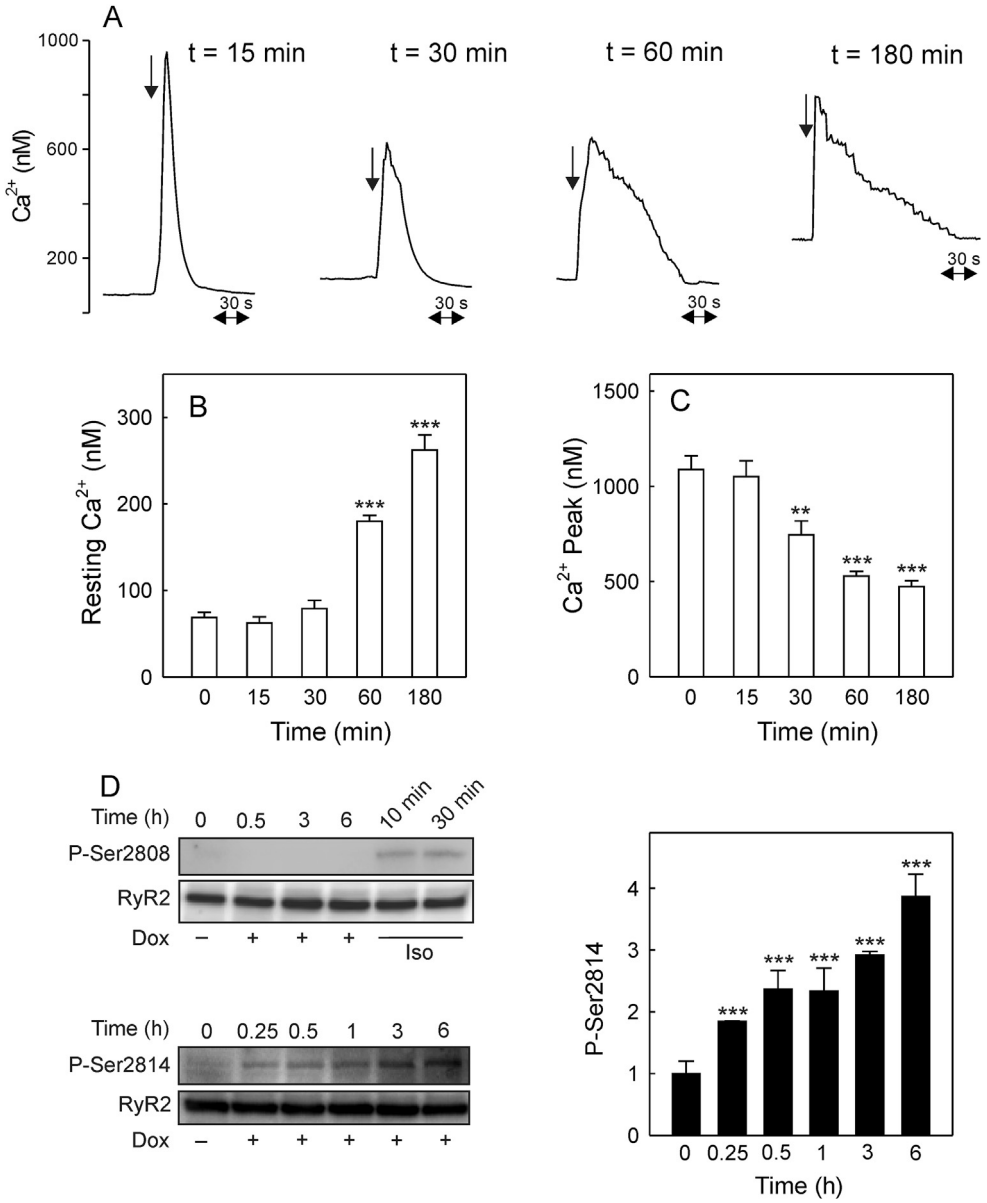

Fig. 2. Doxorubicin effect on cytosolic Ca^{2+} transient induced by caffeine and RyR2 phosphorylation. For Ca^{2+} transient experiments, plated cells were loaded with Fura-3/AM and maintained in Tyrode medium. Data were collected from confocal images of representative cell fields. (A) Ca^{2+} transients induced by 10 mM caffeine (arrow) were recorded at given times after the addition of 5 μM doxorubicin. (B) Evolution of resting Ca^{2+} level during the doxorubicin treatment. *** is $p < 0.001$ vs. control. (C) Caffeine-induced Ca^{2+} peak amplitude at different times when cells were exposed to doxorubicin. ** is $p < 0.01$ vs. control and *** is $p < 0.001$ vs. control. (D) Western blot images and densitometric profile when plated cells maintained in Claycomb medium supplemented with 2 mM L-glutamine were left untreated or exposed to 5 μM doxorubicin (Dox). Time-dependent profiles of RyR2 phosphorylation at Ser2808 (P-Ser2808) or Ser2814 (P-Ser2814) and the corresponding RyR2 levels are shown. Treatment with 1 μM isoproterenol (Iso) was included as positive control of Ser2808 phosphorylation. Densitometry values of P-Ser2814 were normalized against the corresponding RyR2 content and expressed on a relative scale. *** is $p < 0.001$ vs. control.

4. Discussion

Ca^{2+} signaling exhibits significant differences in the myocardiac tissue from different species and also between atrial and ventricular myocytes. Rat atrial myocytes displayed a lower caffeine-induced Ca^{2+} transient and faster decay rate compared to their ventricular counterparts and this was attributed to the higher expression of SERCA2 [9]. When the relative contribution of major Ca^{2+} transporters to Ca^{2+} extrusion was evaluated in HL-1 cells, 70% of cytosolic Ca^{2+} was removed by SERCA (Fig. 1). Therefore, HL-1 cells displayed a lower SERCA contribution (70% *vs.* 92.6%) than atrial myocytes from adult rat [9]. Furthermore, the NCX participation in Ca^{2+} extrusion was lower in HL-1 cells (18% *vs.* 28%) than in non-rodent ventricular myocytes [2] suggesting a distinct intracellular Ca^{2+} regulation.

Ca^{2+} leak from sarcoplasmic reticulum could be caused by RyR activation [23], so the time-dependent rise of diastolic Ca^{2+} and the decrease of caffeine-induced Ca^{2+} peak amplitude (Fig. 2) pointed to RyR as an early target of doxorubicin. RyR2 can be activated by phosphorylation. In fact, Ser2808 is specifically phosphorylated by protein kinase A in mouse, whereas phosphorylation at Ser2814 (first reported to be phosphorylated at Ser2809 in dog [25]), is exclusively accomplished by Ca^{2+}/calmodulin-dependent protein kinase II. Therefore, the selective phosphorylation of RyR2 at

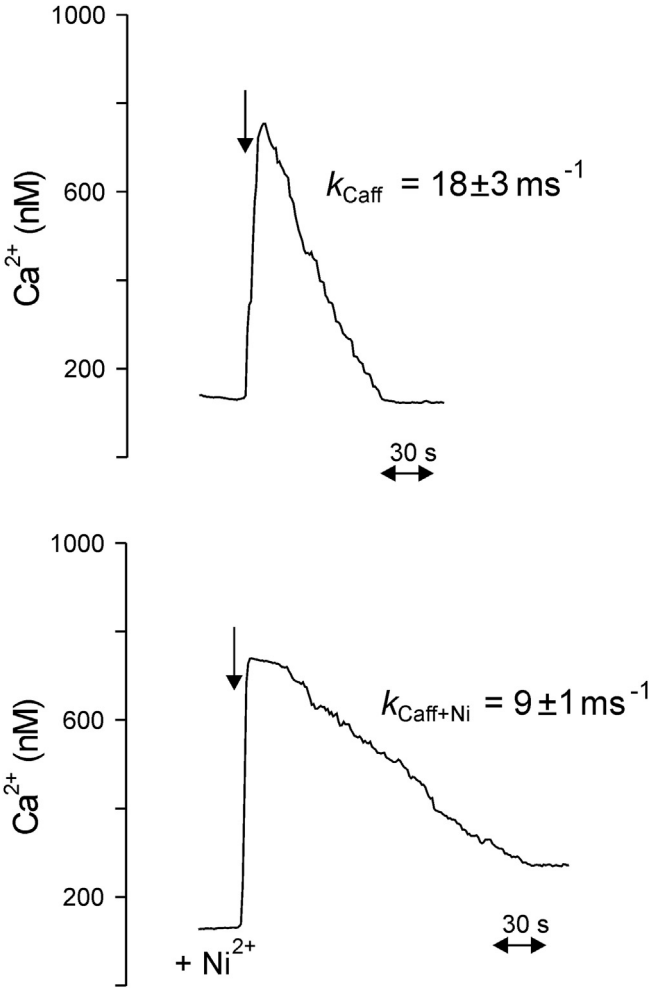

Fig. 3. Evaluation of the doxorubicin effect on NCX. Plated cells were loaded with Fluo-3/AM and maintained in Tyrode medium during the experiments. Top panel: After 1 h treatment with 5 μM doxorubicin, Ca^{2+} transient was induced by adding 10 mM caffeine (arrow) to determine k_{Caff}. Bottom panel: Cells were supplemented with 10 mM $NiCl_2$ and then exposed to 5 μM doxorubicin for 1 h before adding caffeine to evaluate $k_{Caff+Ni}$.

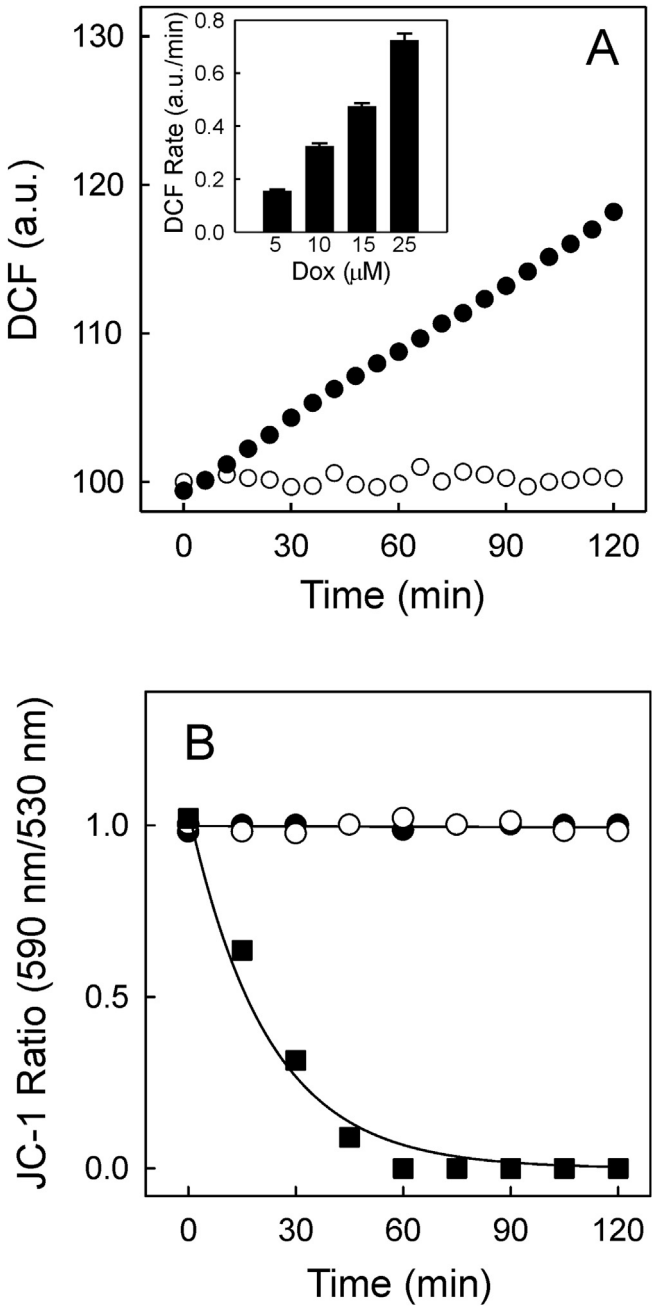

Fig. 4. ROS production and $\Delta\Psi_m$ associated with doxorubicin treatment. Plated cells were loaded with 10 μM H_2-DCFDA and maintained in Tyrode medium. (A) Time-course of DCF fluorescence (a.u.) in a field of cells before (○) or after (●) the addition of 5 μM doxorubicin. Inset of panel A: Dependence of DCF fluorescence rate (a.u./min) on doxorubicin concentration. (B) Cells were loaded with JC-1 and the time-course of the red/green fluorescence was recorded before (○) or after (●) the addition of 5 μM doxorubicin. The time-dependent effect of 5 μM CCCP is included as positive control (■). Data were corrected to discount the fluorescence signal of doxorubicin and energy transfer to JC-1.

Ser2814 revealed the link existing between the activation of this protein kinase II and doxorubicin-induced Ca^{2+} leak [26]. The phosphorylation of RyR2 by Ca^{2+}/calmodulin-dependent protein kinase II, which enhances the resting Ca^{2+} level, has been related with arrhythmias and contractile dysfunction such as those observed in heart failure [27].

Our data also identify a decrease in the caffeine-induced Ca^{2+} transient decay rate during doxorubicin treatment (Fig. 2). In this connection, the slowing [28,29] or acceleration [26] of Ca^{2+} transient decay was reported when rodent cardiomyocytes were exposed to low μM doxorubicin. The distinct behavior can be explained by differences in the cell model and assay conditions, including drug concentration, exposure time and triggering mode of the Ca^{2+} transient. The influence of 5 μM doxorubicin for 1 h on k_{NCX}, as indicator of the NCX activity, revealed an ~11-fold decrease (from 100 to 9 ms^{-1}) with respect to untreated cells (Fig. 3). This effect is consistent with the reported inhibition of Ca^{2+} entry through NCX when measured in isolated heart sarcolemmal vesicles [5]. Therefore, NCX is another early target of short-term doxorubicin treatment and is expected to contribute to diastolic Ca^{2+} overload and the subsequent dysfunction of contractility.

The early accumulation of low doxorubicin concentrations was observed in the nuclei of different cell types while mitochondria were only reached at higher concentrations or longer incubation times [30,31]. In our case, doxorubicin was first accumulated in the mitochondria and not in the nuclei (Fig. 5A), suggesting that doxorubicin location and effect are dependent on concentration, incubation time and even cell type. Even though cardiomyocytes are rich in mitochondria and doxorubicin displays high affinity for the phospholipid cardiolipin [32], no alteration of $\Delta\Psi_m$ by 5 μM

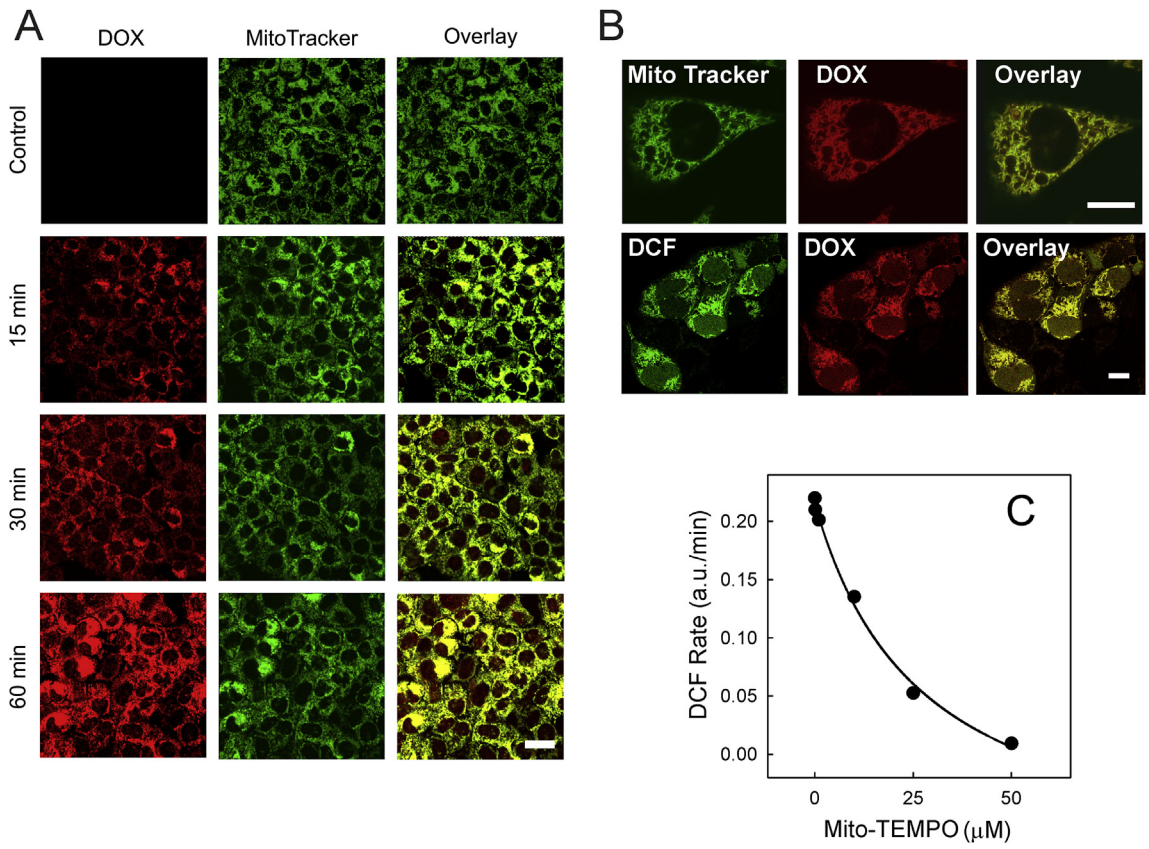

Fig. 5. Intracellular localization of doxorubicin and DCF and mitoTEMPO effect. (A) Plated cells in Tyrode medium and loaded with 150 nM MitoTracker Green were exposed to 5 μM doxorubicin at 37 °C. Confocal images of MitoTracker (green fluorescence) and doxorubicin (red fluorescence) were captured at different time intervals. Bar length is 20 μm. (B) Cells loaded with 5 μM doxorubicin for 15 min were then exposed to H_2-DCFDA for 30 min. Bar length is 10 μm. The colocalization of MitoTracker Green and doxorubicin or DCF and doxorubicin was deduced from the yellow color of overlaid images and was evaluated from the colocalization coefficients. (C) Plated cells loaded with 10 μM H_2-DCFDA and maintained in Tyrode medium were preincubated or not for 1 h with different mitoTEMPO concentrations. The DCF accumulation rate was measured after addition of 5 μM doxorubicin. (For interpretation of the references to color in this figure legend, the reader is referred to the web version of this article.)

doxorubicin was observed during the first 120 min (Fig. 4B). Disruption of the mitochondrial energetic function by 5 μM doxorubicin has been reported to be a late event requiring longer exposure times [33].

The intracellular DCF localization as a ROS probe is also cell type-dependent, i.e., cytosolic in aortic endothelial cells and mitochondrial in adult rat cardiomyocytes [34]. When ROS production was studied in HL-1 cells with the aid of DCF fluorescence, preferential colocalization with doxorubicin was observed (Fig. 5B) and doxorubicin was also seen to colocalize with the mitochondrial probe MitoTracker Green (Fig. 5A and B). This explains why the mitochondrial scavenger mitoTEMPO completely blunted the appearance of ROS (Fig. 5C).

Mitochondrial NOX activity in HL-1 cells and the formation of doxorubicin-induced ROS were both sensitive to inhibition by GKT137831 (Fig. 6). This compound has been demonstrated to be a specific NOX1/NOX4 inhibitor with no ROS scavenging activity [35,36]. Low levels of NOX1 are present at the plasma membrane of resting cardiomyocytes, while NOX4 is abundantly expressed in mitochondria. Besides, mice deficient in NOX activity were resistant to chronic doxorubicin treatment [37]. These data suggest that the one-electron reduction of the doxorubicin quinone ring to give the semiquinone free radical arises from the electron-donor NADPH through mitochondrial NOX activity. It is known that several flavin-containing enzymes, including NOX, in the presence of NADPH may catalyze the one-electron reduction of doxorubicin [38–40]. The rate of ROS production induced by doxorubicin did not decrease but increased by 10% when the mitochondrial complex I was inhibited by 10 μM rotenone (data not shown). The enhancement of superoxide formation when rotenone is added to inhibit the mitochondrial electron transport chain has already been reported [41]. Therefore, mitochondrial ROS generated by electron-donors of the respiratory chain did not contribute to the early oxidative damage induced by doxorubicin in our experimental model and conditions.

Mitochondrial NOX is constitutively active in cardiomyocytes [42], whereas inducible plasma membrane NOX isoforms require the translocation of cytosolic subunits for activation. Our data for HL-1 cells confirm the lack of NOX activity in the microsomal + cytosolic fraction and support the mitochondrial origin of doxorubicin-induced ROS. The superoxide formed from O_2 by reoxidation of the doxorubicin semiquinone is unstable and unable to diffuse across biological membranes but rapidly dismutates to H_2O_2 that is freely permeable. It is conceivable that H_2O_2 diffuses from mitochondria to cytosol where the RyR and NCX targets can be reached.

GKT137831 and melatonin avoided the appearance of ROS after doxorubicin treatment and protected the caffeine-induced Ca^{2+} signal but the mechanisms involved are different. The decrease of the linear rate of ROS production as a function of the GKT137831 concentration added in preincubation (Fig. 7A) is consistent with the inhibition of the mitochondrial NOX activity (Fig. 6A). In contrast, the total inhibition observed at the beginning of doxorubicin-induced ROS after preincubation with melatonin that

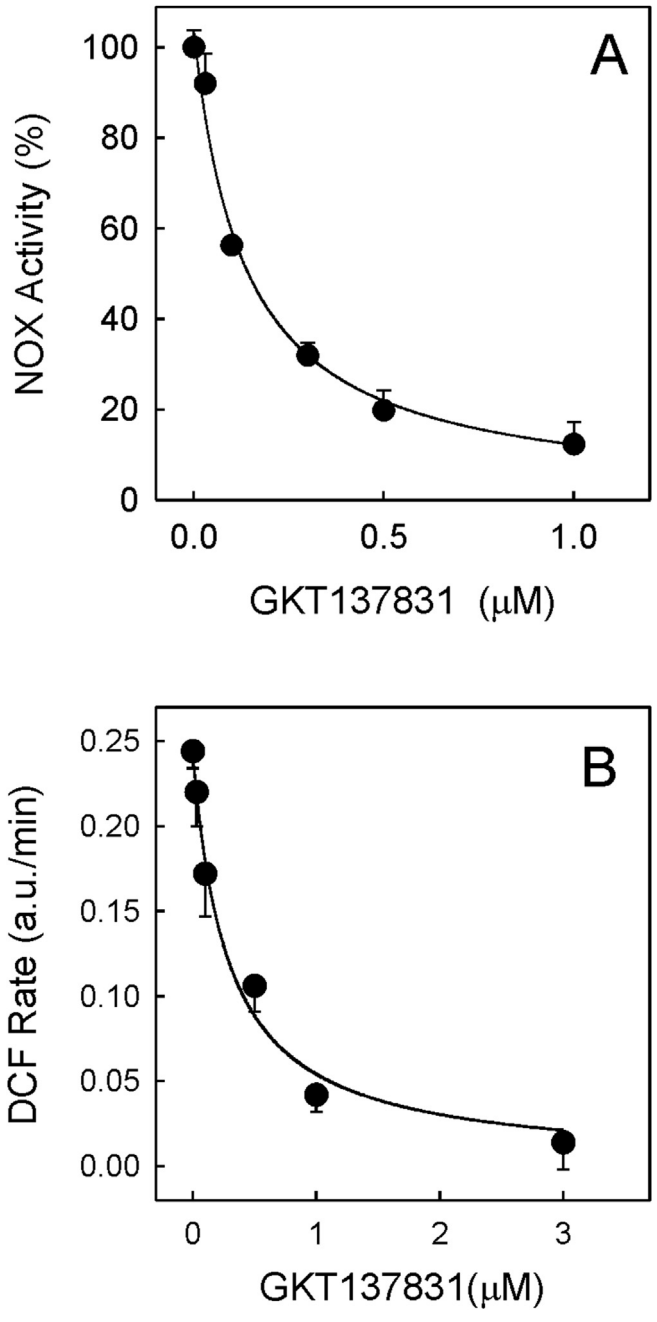

Fig. 6. GKT137831 effect on mitochondrial NOX activity and doxorubicin-induced ROS production. (A) The enzyme activity was studied at 25 °C in a microtiter plate format. The reaction medium was 50 mM KH_2PO_4, pH 7.0, 1 mM EGTA, 150 mM sucrose, 100 μM NADPH, 25 μM lucigenin and 200 μg protein of the mitochondrial fraction in a final volume of 0.2 ml. Different concentrations of GKT137831 were also present when indicated. (B) Plated cells were loaded with 10 μM H_2-DCFDA and maintained in Tyrode medium during the experiments. Cells were preincubated or not for 1 h with different GKT137831 concentrations and the linear rate of DCF accumulation was measured by adding 5 μM doxorubicin.

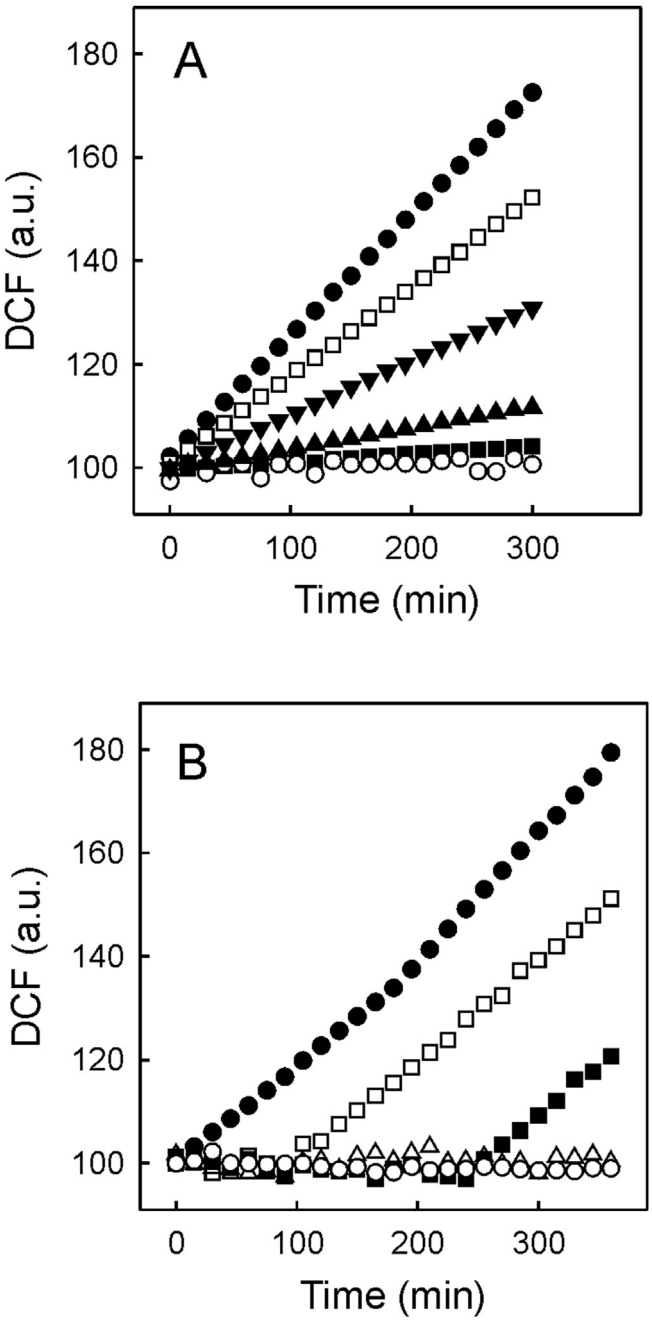

Fig. 7. Protection kinetics against doxorubicin-induced ROS production. Plated cells were loaded with 10 μM H_2-DCFDA and maintained in Tyrode medium during the experiments. (A) Time course of DCF fluorescence when cells were exposed (●) or not (○) to 5 μM doxorubicin. Response when cells were preincubated for 15 min with 0.1 (□), 0.5 (▼), 1 (▲) or 3 μM GKT137831 (■) before doxorubicin was added. (B) Time course of DCF fluorescence when cells were exposed (●) or not (○) to 5 μM doxorubicin. Response when cells were preincubated for 15 min with 10 μM (□), 50 μM (■) or 100 μM (△) melatonin before doxorubicin addition.

was reversed with time (Fig. 7B), is consistent with melatonin consumption due to the ROS scavenging activity [43]. Therefore, mitochondrial NOX inhibition provides permanent protection while ROS scavengers give only temporary protection. This may explain why numerous antioxidant agents efficiently counteracted doxorubicin-induced oxidative damage in cellular models or acute animal experiments but failed in chronic animal treatments or clinical trials. Recent data in NOX4-overexpressing transgenic mice suggest that mitochondrial NOX inhibition by GKT137831 may be a new strategy to prevent/treat myocardiac injuries related with ROS overproduction [44]. In this respect, a phase II clinical trial with diabetic nephropathy patients has been completed (ClinicalTrials.gov Identifier NCT02010242).

ROS overproduction and Ca^{2+} dysregulation are involved in several cardiomyopathies and the question is whether doxorubicin-induced ROS is the cause that altered the Ca^{2+} signal or the

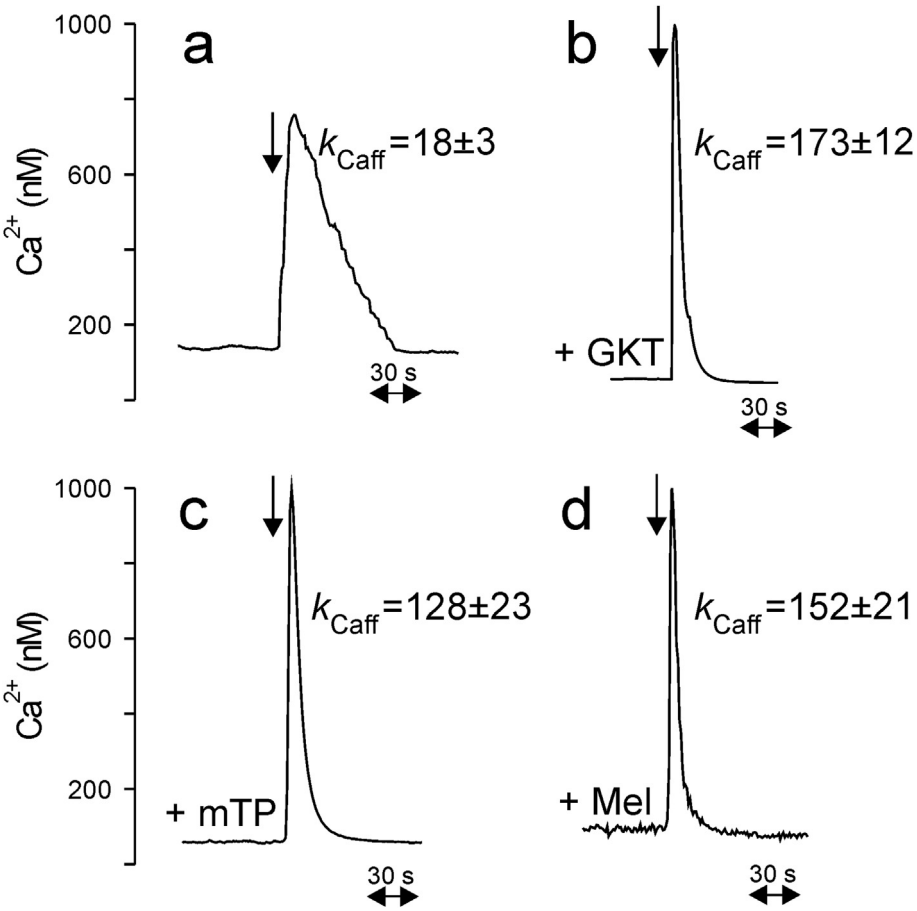

Fig. 8. Protection of Ca^{2+} transporters in cells exposed to doxorubicin. Plated cells loaded with Fluo-3/AM were exposed to 5 μM doxorubicin for 1 h before the addition of 10 mM caffeine (trace a). In similar experiments, cells were preincubated for 1 h with 3 μM GKT137831 (trace b), 50 μM mitoTEMPO (trace c) or 100 μM melatonin (trace d). Representative traces of cytosolic Ca^{2+} signals before or after caffeine addition (arrow) were obtained from a cell field by means of confocal microscopy. k_{Caff} values of Ca^{2+} transient decay ± SEM are expressed in ms^{-1}.

consequence of the Ca^{2+} alteration. When oxidative damage in HL-1 cells was induced by short doxorubicin treatment, the inhibition of ROS production by preincubation with different agents protected the cytosolic Ca^{2+} signal (Fig. 8).

In conclusion, Ca^{2+} transporters related with the systolic Ca^{2+} signal are sensitive to early oxidative damage generated by doxorubicin. ROS production in atrial-derived cardiomyocytes is dependent on mitochondrial NOX activity and, unlike ROS scavengers, permanent protection against oxidative damage can be achieved by limiting the mitochondrial NOX activity.

Conflict of interest

On behalf of all authors, the corresponding author states that there is no conflict of interest.

Acknowledgments

This study was supported in part by Grant FFIS/CM10/011 from Fundación CajaMurcia, Murcia, Spain. We thank Dr. William C. Claycomb from the Louisiana State University Medical Center at New Orleans, LA, for the kindly gift of HL-1 cells and Dr. María García from Servicio de Análisis de Imágenes from our University for technical assistance in quantitative colocalization of fluorescence.

References

[1] M.D. Bootman, D.R. Higazi, S. Coombes, H.L. Roderick, Calcium signalling during excitation-contraction coupling in mammalian atrial myocytes, J. Cell Sci. 119 (2006) 3915–3925.
[2] C.J. Fearnley, H.L. Roderick, M.D. Bootman, Calcium signaling in cardiac myocytes, Cold Spring Harb. Perspect. Biol. 3 (2011) a004242.
[3] P.K. Singal, C.M. Deally, L.E. Weinberg, Subcellular effects of adriamycin in the heart: a concise review, J. Mol. Cel. Cardiol. 19 (1987) 817–828.
[4] G. Minotti, P. Menna, E. Salvatorelli, G. Cairo, L. Gianni, Anthracyclines: molecular advances and pharmacologic developments in antitumor activity and cardiotoxicity, Pharmacol. Rev. 56 (2004) 185–229.
[5] P. Caroni, F. Villani, E. Carafoli, The cardiotoxic antibiotic doxorubicin inhibits the Na^+/Ca^{2+} exchange of dog heart sarcolemmal vesicles, FEBS Lett. 130 (1981) 184–186.
[6] S.R.M. Holmberg, A.J. Williams, Patterns of interaction between anthraquinone drugs and the calcium-release channel from cardiac sarcoplasmic reticulum, Circ. Res. 67 (1990) 272–283.
[7] E.C. Keung, L. Toll, M. Ellis, R.A. Jensen, L-Type cardiac calcium channels in doxorubicin cardiomyopathy in rats morphological, biochemical and functional correlations, J. Clin. Invest. 87 (1991) 2108–2113.
[8] M. Arai, K. Tomaru, T. Takizawa, K. Sekiguchi, T. Yokoyama, T. Suzuki, R. Nagai, Sarcoplasmic reticulum genes are selectively down-regulated in cardiomyopathy produced by doxorubicin in rabbits, J. Mol. Cell Cardiol. 30 (1998) 243–254.
[9] A.P. Walden, K.M. Dibb, A.W. Trafford, Differences in intracellular calcium homeostasis between atrial and ventricular myocytes, J. Mol. Cell Cardiol. 46 (2009) 463–473.
[10] W.C. Claycomb, N.A. Lanson Jr., B.S. Stallworth, D.B. Egeland, J.B. Delcarpio, A. Bahinski, N.J. Izzo Jr., HL-1 cells: A cardiac muscle cell line that contracts and retains phenotypic characteristics of the adult cardiomyocyte, Proc. Natl. Acad. Sci. U. S. A. 95 (1998) 2979–2984.
[11] M. Barriga, R. Cal, N. Cabello, A. Llach, A. Vallmitjana, R. Benítez, L. Badimon, J. Cinca, V. Llorente-Cortés, L. Hove-Madsen, Low density lipoproteins

promote unstable calcium handling accompanied by reduced SERCA2 and connexin-40 expression in cardiomyocytes, PLoS One 8 (2013), 3e58128.
[12] M.C. Asensio-López, A. Lax, D.A. Pascual-Figal, M. Valdés, J. Sánchez-Más, Metformin protects against doxorubicin-induced cardiotoxicity: involvement of the adiponectin cardiac system, Free Radic. Biol. Med. 51 (2011) 1861–1871.
[13] L. Gianni, L. Vigano, A. Locatelli, G. Capri, A. Giani, E. Tarenzi, G. Bonadonna, Human pharmacokinetic characterization and in vitro study of the interaction between doxorubicin and paclitaxel in patients with breast cancer, J. Clin. Oncol. 15 (1997) 1906–1915.
[14] F. Soler, A. Lax, M.C. Asensio, D. Pascual-Figal, F. Fernandez-Belda, Passive Ca^{2+} overload in H9c2 cardiac myoblasts: assessment of cellular damage and cytosolic Ca^{2+} transients, Arch. Biochem. Biophys. 512 (2011) 175–182.
[15] G. Grynkiewicz, M. Poenie, R.Y. Tsien, A new generation of Ca^{2+} indicators with greatly improved fluorescence properties, J. Biol. Chem. 260 (1985) 3440–3450.
[16] N. Negretti, S.C. O'Neill, D.A. Eisner, The relative contributions of different intracellular and sarcolemmal systems to relaxation in rat ventricular myocytes, Cardiovasc Res. 27 (1993) 1826–1830.
[17] M.R. Fowler, J.R. Naz, M.D. Graham, G. Bru-Mercier, S.M. Harrison, C.H. Orchard, Decreased Ca^{2+} extrusion via Na^{+}/Ca^{2+} exchange in epicardial left ventricular myocytes during compensated hypertrophy, Am. J. Physiol. Heart Circ. Physiol. 288 (2005) H2431–H2438.
[18] M.C. Asensio-López, J. Sánchez-Más, D.A. Pascual-Figal, S. Abenza, M.T. Pérez-Martínez, M. Valdés, A. Lax, Involvement of ferritin heavy chain in the preventive effect of metformin against doxorubicin-induced cardiotoxicity, Free Radic. Biol. Med. 57 (2013) 188–200.
[19] A.R. Rosenkranz, S. Schmaldienst, K.M. Stuhlmeier, W. Chen, W. Knapp, G.J. Zlabinger, A microplate assay for the detection of oxidative products using 2′,7′-dichlorofluorescein-diacetate, J. Immunol. Methods 156 (1992) 39–45.
[20] M. Reers, T.W. Smith, L.B. Chen, J-aggregate formation of a carbocyanine as a quantitative fluorescent indicator of membrane potential, Biochemistry 30 (1991) 4480–4486.
[21] E.M.M. Manders, F.J. Verbeek, J.A. Aten, Measurement of co-localization of objects in dual-colour confocal images, J. Microsc. 169 (1993) 375–382.
[22] K.K. Griendling, C.A. Minieri, J.D. Ollerenshaw, R.W. Alexander, Angiotensin II stimulates NADH and NADPH oxidase activity in cultured vascular smooth muscle cells, Circ. Res. 74 (1994) 1141–1148.
[23] T.R. Shannon, K.S. Ginsburg, D.M. Bers, Quantitative assessment of the SR Ca^{2+} leak-load relationship, Circ. Res. 91 (2002) 594–600.
[24] A.E. Dikalova, A.T. Bikineyeva, K. Budzyn, R.R. Nazarewicz, L. McCann, W. Lewis, D.G. Harrison, S.I. Dikalov, Therapeutic targeting of mitochondrial superoxide in hypertension, Circ. Res. 107 (2010) 106–116.
[25] D.R. Witcher, R.J. Kovacs, H. Schulman, D.C. Cefali, L.R. Jones, Unique phosphorylation site on the cardiac ryanodine receptor regulates calcium channel activity, J. Biol. Chem. 266 (1991) 11144–11152.
[26] C.M. Sag, A.C. Köhler, M.E. Anderson, J. Backs, L.S. Maier, CaMKII-dependent SR Ca leak contributes to doxorubicin-induced impaired Ca handling in isolated cardiac myocytes, J. Mol. Cell Cardiol. 51 (2011) 749–759.
[27] X. Ai, J.W. Curran, T.R. Shannon, D.M. Bers, S.M. Pogwizd, Ca^{2+}/calmodulin-dependent protein kinase modulates cardiac ryanodine receptor phosphorylation and sarcoplasmic reticulum Ca^{2+} leak in heart failure, Circ. Res. 97 (2005) 1314–1322.
[28] A. Maeda, M. Honda, T. Kuramochi, T. Takabatake, A calcium antagonist protects against doxorubicin-induced impairment of calcium handling in neonatal rat cardiac myocytes, Jpn. Circ. J. 63 (1999) 123–129.
[29] A. Berdichevski, G. Meiry, F. Milman, I. Reiter, O. Sedan, S. Eliyahu, H.S. Duffy, M.B. Youdim, O. Binah, TVP1022 protects neonatal rat ventricular myocytes against doxorubicin-induced functional derangements, J. Pharmacol. Exp. Ther. 332 (2010) 413–420.
[30] M. Tokarska-Schlattner, M. Zaugg, R. da Silva, E. Lucchinetti, M.C. Schaub, T. Wallimann, U. Schlattner, Acute toxicity of doxorubicin on isolated perfused heart: response of kinases regulating energy supply, Am. J. Physiol. Heart Circ. Physiol. 289 (2005) H37–H47.
[31] J. Savatier, T. Rharass, C. Canal, A. Gbankoto, J. Vigo, J.-M. Salmon, A.-C. Ribou, Adriamycin dose and time effects on cell cycle, cell death, and reactive oxygen species generation in leukaemia cells, Leuk. Res. 36 (2012) 791–798.
[32] E. Goormaghtigh, P. Chatelain, J. Caspers, J.M. Ruysschaert, Evidence of a specific complex between adriamycin and negatively-charged phospholipids, Biochim. Biophys. Acta 597 (1980) 1–14.
[33] M.C. Asensio-Lopez, J. Sanchez-Mas, D.A. Pascual-Figal, C. de Torre, M. Valdes, A. Lax, Ferritin heavy chain as main mediator of preventive effect of metformin against mitochondrial damage induced by doxorubicin in cardiomyocytes, Free Radic. Biol. Med. 67 (2014) 19–29.
[34] L.M. Swift, N. Sarvazyan, Localization of dichlorofluorescin in cardiac myocytes: implications for assessment of oxidative stress, Am. J. Physiol. Heart Circ. Physiol. 278 (2000) H982–H990.
[35] B. Laleu, F. Gaggini, M. Orchard, L. Fioraso-Cartier, L. Cagnon, S. Houngninou-Molango, A. Gradia, G. Duboux, C. Merlot, F. Heitz, C. Szyndralewiez, P. Page, First in class, potent, and orally bioavailable NADPH oxidase isoform 4 (Nox4) inhibitors for the treatment of idiopathic pulmonary fibrosis, J. Med. Chem. 53 (2010) 7715–7730.
[36] T. Aoyama, Y.-H. Paik, S. Watanabe, B. Laleu, F. Gaggini, L. Fioraso-Cartier, S. Molango, F. Heitz, C. Merlot, C. Szyndralewiez, P. Page, D.A. Brenner, Nicotinamide adenine dinucleotide phosphate oxidase in experimental liver fibrosis: GKT137831 as a novel potential therapeutic agent, Hepatology 56 (2012) 2316–2327.
[37] L. Wojnowski, B. Kulle, M. Schirmer, G. Schlüter, A. Schmidt, A. Rosenberger, S. Vonhof, et al., NAD(P)H oxidase and multidrug resistance protein genetic polymorphisms are associated with doxorubicin-induced cardiotoxicity, Circulation 112 (2005) 3754–3762.
[38] A. Bartoszek, C.R. Wolf, Enhancement of doxorubicin toxicity following activation by NADPH cytochrome P450 reductase, Biochem. Pharmacol. 43 (1992) 1449–1457.
[39] J. Vásquez-Vivar, P. Mártasek, N. Hogg, B.S. Masters, K.A. Pritchard Jr., B. Kalyanaraman, Endothelial nitric oxide synthase-dependent superoxide generation from adriamycin, Biochemistry 36 (1997) 11293–11297.
[40] M. Gilleron, X. Marechal, D. Montaigne, J. Franczak, R. Neviere, S. Lancel, NADPH oxidases participate to doxorubicin-induced cardiac myocyte apoptosis, Biochem. Biophys. Res. Commun. 388 (2009) 727–731.
[41] H. Pelicano, L. Feng, Y. Zhou, J.S. Carew, E.O. Hileman, W. Plunkett, M.J. Keating, P. Huang, Inhibition of mitochondrial respiration: a novel strategy to enhance drug-induced apoptosis in human leukemia cells by a reactive oxygen species-mediated mechanism, J. Biol. Chem. 278 (2003) 37832–37839.
[42] T. Ago, J. Kuroda, J. Pain, C. Fu, H. Li, J. Sadoshima, Upregulation of Nox4 by hypertrophic stimuli promotes apoptosis and mitochondrial dysfunction in cardiac myocytes, Circ. Res. 106 (2010) 1253–1264.
[43] R.J. Reiter, D.X. Tan, J. Cabrera, D. D'Arpa, Melatonin and tryptophan derivatives as free radical scavengers and antioxidants, Adv. Exp. Med. Biol. 467 (1999) 379–387.
[44] Q.D. Zhao, S. Viswanadhapalli, P. Williams, Q. Shi, C. Tan, X. Yi, B. Bhandari, H.E. Abboud, NADPH oxidase 4 induces cardiac fibrosis and hypertrophy through activating Akt/mTOR and NFκB signaling pathways, Circulation 131 (2015) 643–655.